Strathclyde Engagement with the National HVDC Centre: Phase I Converter and GB Network Modelling

Doc. Type:	Technical report	*Date:*	**31/10/2018**
Doc. N°:	**USTRATH-HVDC Centre-P1-005**	*Issue:* **5**	*Page:* **1** *of* **17**
Title:	DC Grid with User-defined Converter Models: Validation of Real-Time Model in RTDS against Offline Equivalents in PSCAD/EMTDC Environment		

	Name & Function	*Signature*	*Date*
Prepared by:	Deyang Guo, Md Habibur Rahman, Grain P Adam, Abdullah Emhemed		28/10/2018
Approved by:	Lie Xu		31/10/2018
Authorized by:	Yash Audichya		

DISTRIBUTION LIST	N	A	I
Internal			
External			

N=Number of copy
A=Application
I=Information

TABLE OF CONTENT

Executive summary

Previous studies have developed and validated several user-defined MMC and hybrid models by comparing real-time results with the offline models, considering one converter terminal. These reports have established that the averaged models of the half-bridge,full-bridge, and hybrid MMCs are able to produce practically identical results as the Thevenin Equivalent and Switching function models during normal operation and AC/DC faults. On this basis, Report IV has demonstrated the suitability of the offline user-defined HB-MMC models for DC grid studies. As a follow up to these previous studies, this report demonstrates the suitability of the developed converter models and associated control systems for complex DC grid studies, where the results of offline simulation platform and have been corroborated against that of real-time simulation platform. The benchmarking of the simulation waveforms in the two simulation platforms shows that they produce practically identical results. It further validates the use of different DC voltage control strategies on active power regulation and maintaining DC power balancing, and DC voltage control during both normal and abnormalfault conditions.

1 Introduction

In recent years, DC grids have been recognized as and one of the platforms that would facilitate maximum utilization of electricity generated from various renewable energy resources with the power plants dispersed over wide geographical areas, benefiting from the diversity of seasons and weather patterns. DC grids also provide means to efficiently exchange large power over long distances, bypassing bottlenecks and congestion points of the conventional HVAC grids.

The ability to instantly sink and source DC power in order to maintain power balance in multi-terminal DC grids makes the voltage source converter (VSC) as a preferred technology for DC grid, with modular multilevel converter (MMC) and its variants are the more likely topologies to be adopted. Evidently, a number of projects have already been commissioned in China [1-3], though significant outstanding technical challenges yet to be addressed (such as lack of generic and cost-effective strategies for DC fault handling in critical power corridor regardless of DC grid topology, and means to manage power flow within highly complex meshed DC grid with the aim of preventing DC cables overload and ensure efficient operation o overall system).

Ideally, communication is not required between converter terminals, especially, during normal operating conditions as local controllers at each converter stations will be sufficient to ensure stable operation of the DC grid, with high-level DC controllers only needed to enhance and optimize utilization of transmission infrastructures [4-6]. Because of the vulnerability of semiconductors to high current stresses, converter stations cannot rely on communication based protection. Instead, protection system based on local measurements is preferred.

The previous reports have validated a number of user-defined real-time and offline MMC models, with all previous validations have been performed on one converter terminal. Report III [7] has demonstrated the suitability of the offline user-defined models for DC grid studies. Therefore, this report aims to demonstrate the suitability of these models for complex DC grid studies in offline and real-time platforms, on the basis of one-to-one validation between PSCAD and RTDS simulation waveforms. The benchmarking of the real-time waveforms versus offline counterparts have shown that the models developed in the two platforms are equivalents and produce practically identical results, with the offline offers cheaper simulation solutions, and real-time offers highly interactive co-simulation solutions that can accommodate real-world hardware, controllers and protection systems.

2 System Description

Fig. 1 shows a three-terminal symmetrical monopole DC grid with ±320 kV DC voltage and three half-bridge modular multilevel converters MMC_1, MMC_2 and MMC_3. The two converter terminals MMC_1 and MMC_2 are connected to weak and strong AC grids with SCR=2.5 and SCR=15, respectively. The largest converter terminal MMC_2 which is connected to the strongest AC grid is designated to operate as a DC voltage controlling converter. MMC_3 is connected to a wind farm with load connected to the local network. It is controlled as grid forming converter in order to establish stiff AC voltage at the wind farm and to absorb the net active power generated by the wind farm and provide the required reactive power in the wind farm AC network. Detailed system parameters of the DC grid to be studied are shown in Fig. 1. For

simulation efficiency, all converter terminals and the wind farm in the DC grid shown in Fig. 1 are modelled in PSCAD and RTDS using averaged models, and all DC and AC cables are represented by lumped parameter π models.

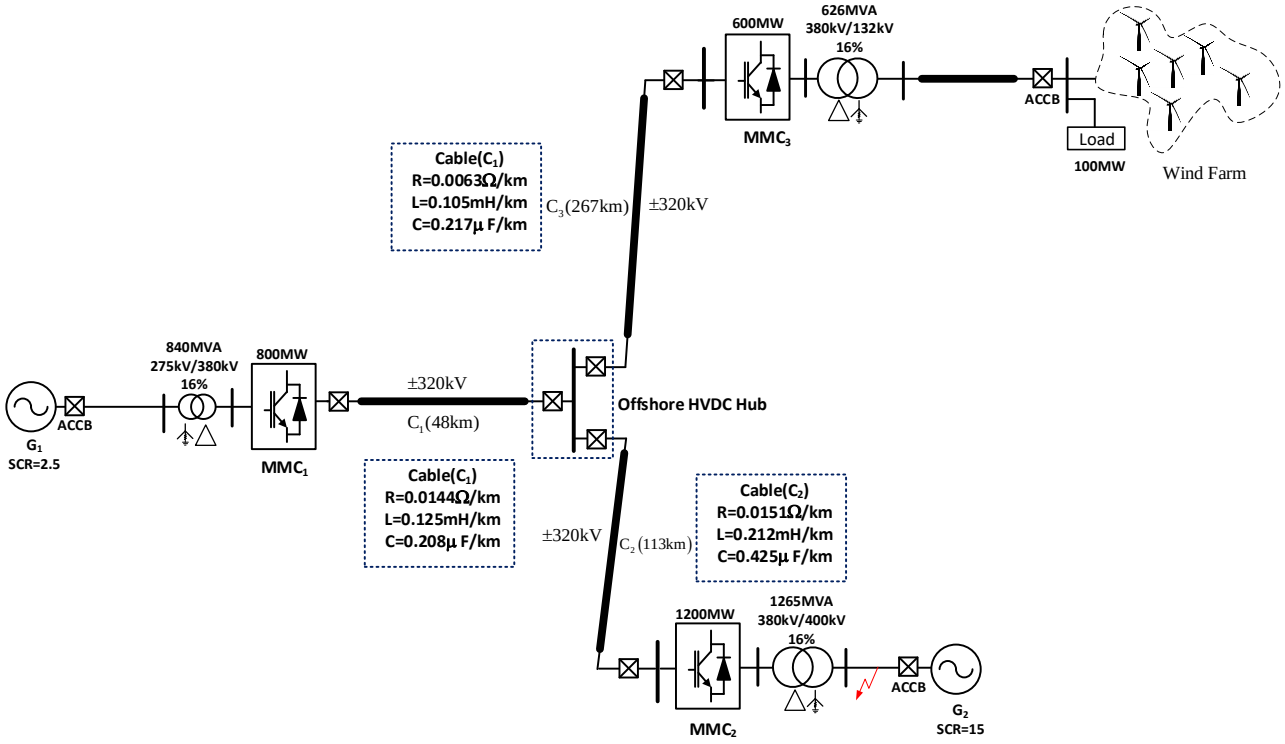

Fig. 1: Block diagram of a three-terminal MMC based DC grid

2.1 Modelling of Converter Terminals

The HB-MMC averaged model employed to represent MMC_1, MMC_2 and MMC_3 in PSCAD and RSCAD environments have already been extensively validated. These models have an identical structure of the inner controllers, i.e., positive and negative sequence current controllers in d-q, per phase proportional resonant circulating current controllers, and vertical and horizontal capacitor voltage balancing controllers. The outer controllers on d and q axes of the MMC_2 regulate DC voltage and reactive power, while the outer controllers on d and q axes of the MMC_3 regulate direct and quadrature components of the AC voltage in the offshore AC network so as to operate as a grid forming converter. In the MMC_1, the outer controller on q-axis regulates AC voltage magnitude at the point of common coupling, while the outer controller on d-axis of the MMC_1 has been tested under the following settings:

1) Conventional active power controller.
2) DC voltage droop control based on V-I characteristics shown in Fig. 2.
3) P-Vdc droop shown in Fig. 3.

Detailed explanations of different droop methods in Fig. 2 and Fig. 3 were presented in Report III [7].

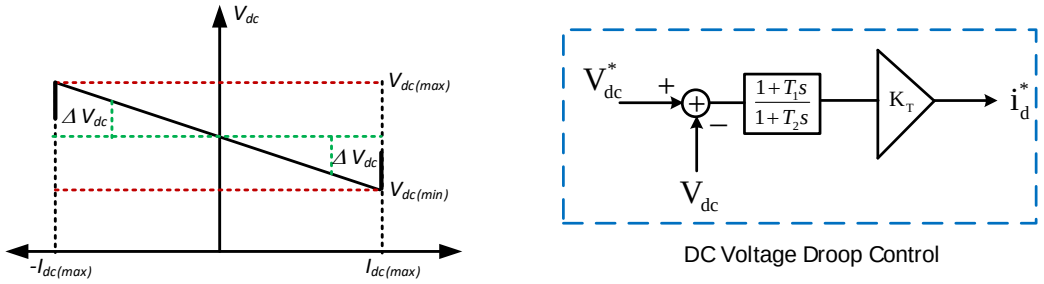

(a) (b)

Fig. 2: Droop Method 1: (a) DC V-I droop characteristic (b) DC voltage droop control

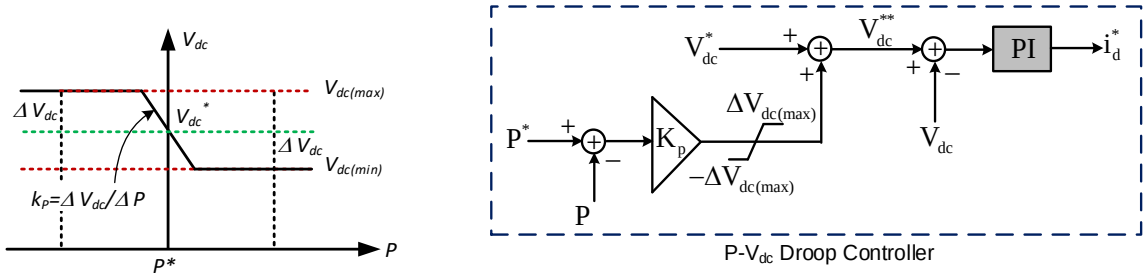

(a) (b)

Fig. 3: Droop Method 2: (a) P-V_{dc} droop characteristic, (b) P-V_{dc} droop controller

2.2 Modelling of Wind Farm

The wind farm connected to MMC_3 is represented by an aggregated averaged model of the grid side converter described in Report III [7]. The main focus this project is on HVDC and wind turbine converter modelling, and studies of interests in this report fall within the short time-scale of electromagnetic transients. Thus, the detailed wind farm/turbine dynamics have no bearing on the accuracy of the results. This is because in such time-scale the mechanical input torques of the wind generators remain constant. The main controllers incorporated in the wind farm model are active and reactive power controllers, and inner current controllers.

Fig. 4 shows the overall control structure of the wind farm grid side converter and MMC_3 converter. MMC_3 that connects the wind farm to the DC grid adopts the same inner control systems as MMC_1 and MMC_2 with the addition of outer AC voltage control loop. The wind farm converter controls its active and reactive powers according to the set-points.

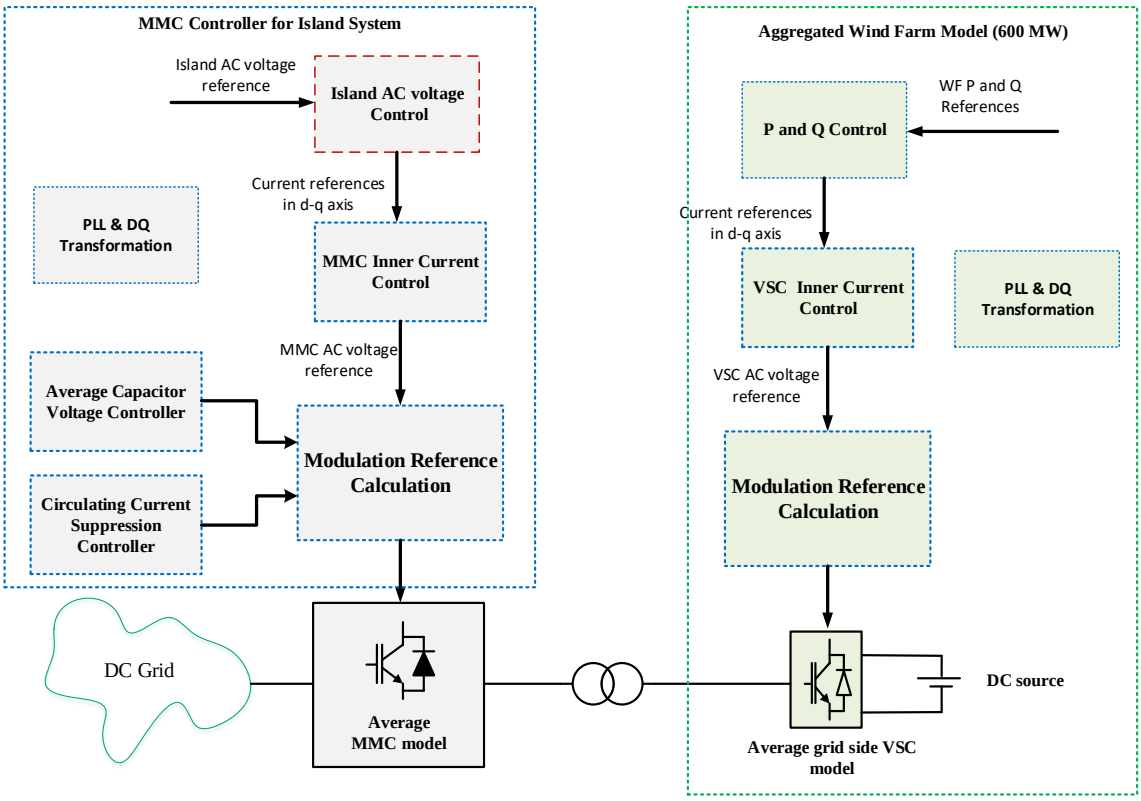

Fig. 4: An aggregated wind farm connected with MMC converter and control diagrams of the wind farm grid side converter and MMC converter

2.3 System Parameters

Table 1, Table 2 and Table 3 summarise parameters of the MMC_1, MMC_2 and MMC_3 and the wind farm.

Table 1: System parameters (AC Side)

Item	MMC_1	MMC_2	MMC_3
Rated Apparent Power (S)	840 MVA	1265 MVA	626 MVA
Rated Active Power (P)	±800 MW	±1200 MW	±600 MW
Converter Nominal DC Voltage	640 kV (±320 kV)	640 kV (±320 kV)	640 kV (±320 kV)
Converter Nominal AC Voltage	380 kV	380 kV	380 kV
AC Grid Voltage	275 kV	400 kV	132 kV
Nominal Frequency	50 Hz	50 Hz	50 Hz
SCR	2.5	15	-
X/R Ratio	10	10	10
Transformer Rated Apparent Power	840 MVA	1265 MVA	626 MVA
Transformer Voltage Ratio	275/380 kV	400/380 kV	132/380 kV
Transformer Reactance	0.16 pu	0.16 pu	0.16 pu

Table 2: Wind farm System parameters

Item	Wind farm (WF)
Rated Apparent Power (S)	626 MVA
Rated Active Power (P)	±600 MW
Converter Nominal DC Voltage	1.2 kV
Converter Nominal AC Voltage	0.69 kV
AC Grid Voltage	132 kV
Nominal Frequency	50 Hz
Transformer Rated Apparent Power	840 MVA
Transformer Voltage Ratio	132/0.69 kV
Transformer Reactance	0.16 pu
Local Load	100 MW

Table 3: System parameters (MMC)

Item	MMC $_1$	MMC $_2$	MMC $_3$
Arm inductance	13%	13%	13%
Number of cells per arm (N)	350	350	350
Cell Capacitance	7.2 mF	10.8mF	5.4mF
Average Cell capacitance	20.55 µF	30.83 μF	15.4 μF

2.4 RTDS implementation

The DC grid shown in Fig. 1 is implemented in RTDS using the concept of multi-rate, with two distinct sampling times. The power circuits of the three converters and DC cables are placed in 3 processors on GPC cards that operate at 2.5µs time step. Whilst the two AC grids, wind farm, control systems and parts that describe the dynamics of the averaged converter models operate at 50µs time step. Two AC sources that represent the AC grids are placed in one processor on the GPC card. The AC sides of the MMC_1 and MMC_2 that operate at 2.5µs (small) time-steps are interfaced to the AC grids that operate at 50µs (large) time-step via two interfacing transformers. Similarly, the wind farm operates at 50µs time step is connected to the AC side of MMC_3 that operates at 2.5µs (small) time-step via another interfacing transformer. The DC sides of the converter models and their associate DC cables that operate at small time step but different processors are linked together through a short T-lines to form a DC grid.. It is worth stressing that the uses of T-lines for connecting converter models and DC cables that operate on different processors and interfacing transformers for connecting system components that operate with different sample times are commonly used practice in RTDS and have a negligible impact on the accuracy of the real-time simulation results as it will be demonstrated later.

3 Simulations

This section uses real-time and offline simulations performed using RSCAD/RTDS and PSCAD/EMTDC to assess the followings:

1) The performance of the DC grid in Fig. 1 when it is operating under normal and abnormal operating conditions summarised in Table 4 including AC faults.

2) The suitability of the developed user-defined offline and real-time MMC models for DC grid simulations.

Table 4: Summary of the operating conditions and simulation scenarios, with the AC side of the MMC_2 is subjected to a symmetrical three-phase AC fault at t=7s in scenarios II and III only

Operating Scenarios		**I**	**II**	**III**
		Conventional method	**Droop method 1**	**Droop method 2**
AC Fault		No	Yes	Yes
MMC_1	**Control objectives**	P and Q	V_{dc} Droop and Q	P-V Droop and Q
	Condition	P= 400 MW V_{ac}=275 kV	V_{dc}= 646 kV V_{ac}=275 kV	P= 400 MW V_{ac}=275 kV
MMC_2	**Control objectives**	V_{dc} and Q		
	Condition	V_{dc}= 640 kV, Q=300 MVAr		
MMC_3	**Control objectives**	V_d =107.78 kV and V_q=0 (V_{ac}=132kV line-to-line RMS)		
	Condition	Islanded Mode		

3.1 Scenario I: Conventional control method

This section examines the performance of the DC grid in Fig. 1 when MMC_1 controls active power and AC voltage, MMC_2 controls V_{dc} and Q, and MMC_3 operates as grid forming converter for the wind farm as described earlier and shown in Table 4. Fig. 5 shows simulation waveforms when the DC grid operates under the conventional control method, with the set-points of the stations MMC_1, MMC_2 and MMC_3 as follows:

- Initially, MMC_1 controls active power at 0, and at t=5.5s, it varies active power from 0 to 400 MW at a rate of 800 MW/s. From start, MMC_1 constantly controls its local AC voltage at 275 kV (line-to-line).
- MMC_2 controls DC voltage at 640 kV (pole-to-pole), and at t=2.5 s, it ramps up its reactive power output from 0 MVAr to 300 MVAr at a rate of 600 MVAr/s.
- At the start, the local AC network connected to MMC_3 is de-energised, and at t=1.5 s, MMC_3 starts building up the AC voltage from 0 to rated value of 132 kV within 0.5 s.
- Wind farm (WF) connected to MMC_3, start ramps its active power from zero to 250 MW at 2.5 s at a rate of 500 MW/s. At t=4.5 s, it ramps its power up from 250 MW to 500 MW at a rate of 1000 MW/s. At t=2.5s, the WF also ramps up its reactive power output from 0 to 100 MVAr at a rate of 200 MVAr/s.

Under the conventional control method and operation conditions summarised above, Fig. 5 (a), (b), (c) and (d) show the real-time simulation waveforms of active and reactive powers of the MMC_1, MMC_2 and MMC_3 and the wind farm (WF) overlaid on the offline counterparts. Positive directions of active and

reactive powers are from AC grids toward converters in both MMCs and wind farm. Notice that the MMC_3 has to supply the local load of 100 MW when the wind farm outputs zero power, and after the increase of wind farm power generation, the net power export from MMC_3 to the DC grid is always less than the wind farm power by 100MW (power consumption in the local load).

Fig. 5 (e), (f) and (g) display the DC voltages, DC currents and R.M.S values of the line-to-line AC voltages of the MMC_1, MMC_2 and MMC_3 measured at the grid side. These waveforms show that the real-time DC grid model simulated in RTDS produces practically identical results as its offline PSCAD equivalent. The offline and real-time simulation traces of the instantaneous AC voltages and currents displayed in Fig. 5 (h), (i), (j) and (k) exhibit a high level of similarities to great detail.

From the simulation waveforms shown in Fig. 5, it can be concluded that the user-defined models being tested in RTDS and PSCAD are in full agreement and in line with the expected results based on theoretical understanding of the voltage source converters in wind and HVDC applications, including the MMCs.

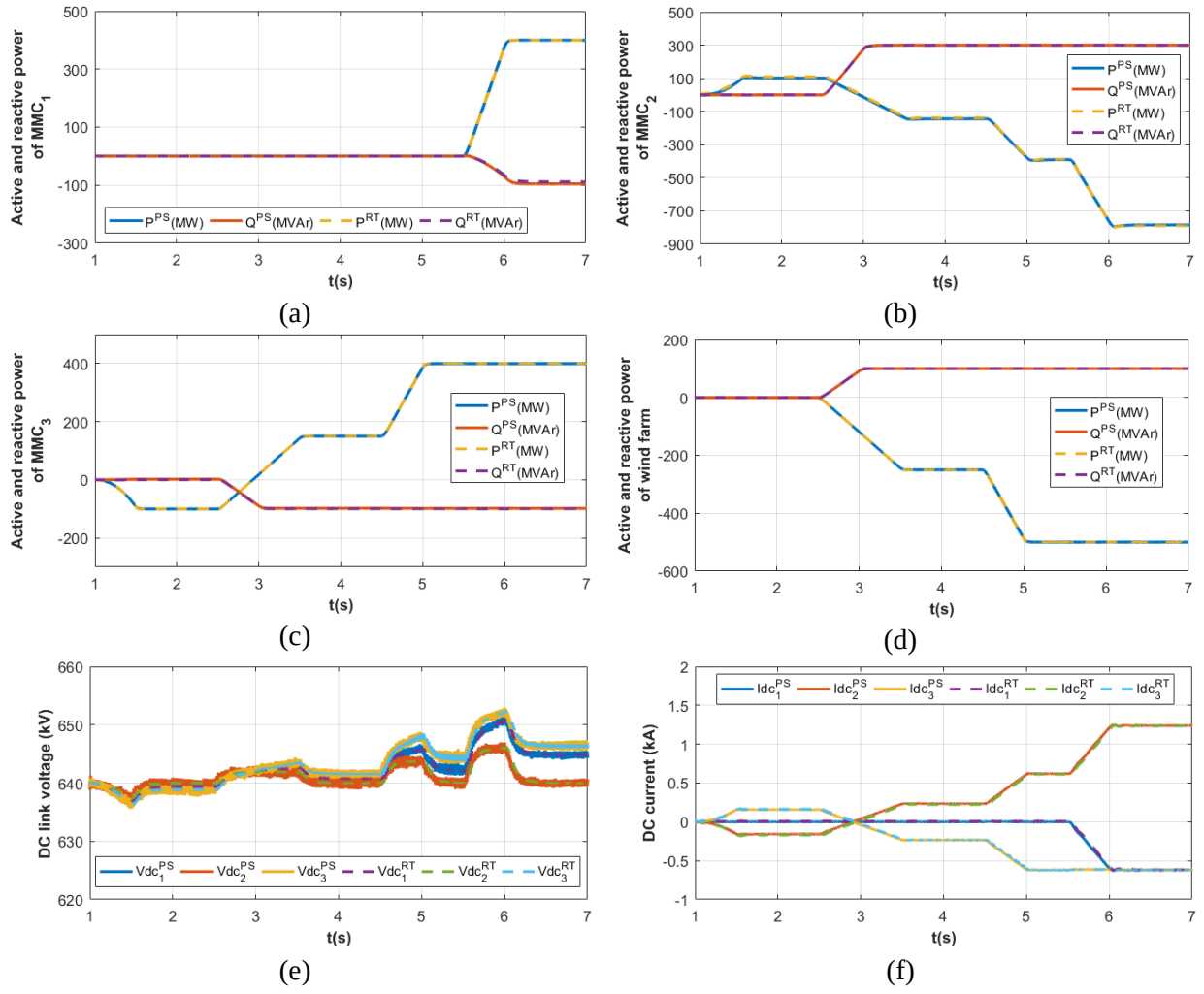

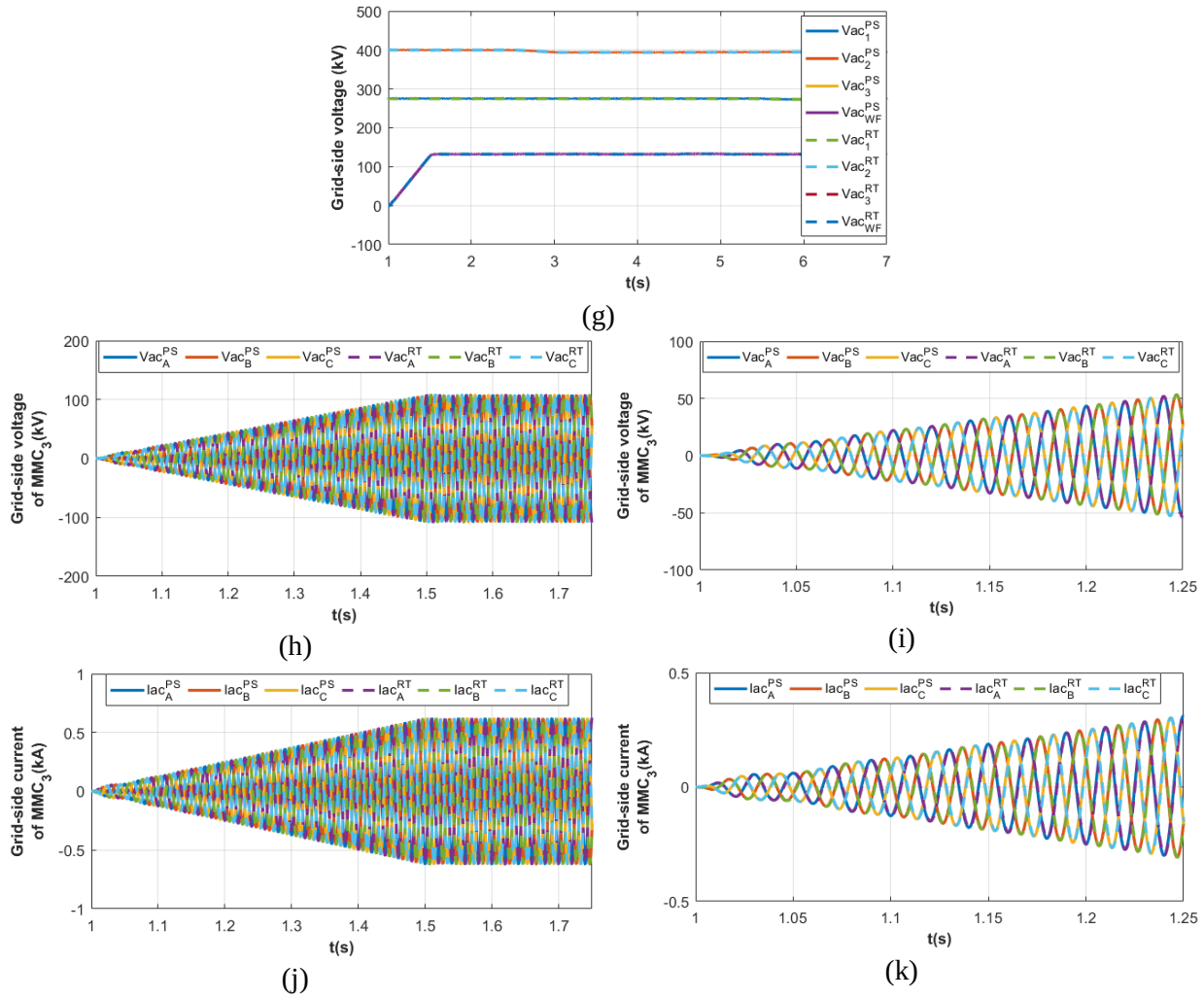

Fig. 5: Simulation waveforms that illustrate the performance of a DC grid during normal operation with real-time traces are superimposed on their equivalents offline traces.

3.2 Scenario II: Droop Control-Method 1

This section presents real-time and offline simulation waveforms when basic DC voltage droop is employed at MMC_1, and AC fault is applied at t=7 s at PCC of the MMC_2. In this scenario, the DC grid operating conditions as follows:

- MMC_1 is equipped with a basic DC voltage-current droop method, denoted as droop control method 1, so that it can adjust its active power according to the DC voltage level. In this case, its DC voltage droop is setup to ensure that at normal operation, the majority of active power being generated by the wind farm to be exported to the G_2, through MMC_2 that operates as DC voltage controlling converter. Also, MMC_1 constantly controls its local AC voltage at 275 kV (line-to-line).
- In pre-fault, MMC_2 uses conventional PI based DC voltage controller to regulate the DC grid DC voltage constantly at 640 kV (pole-to-pole). Also, the MMC_2 maintains its reactive power output constant at +300 MVAr.

- MMC_3 regulates AC voltage at its PCC at 132 kV, while the wind farm outputs -500MW (generation) and +100MVAr.

In this scenario, an AC fault is applied in the PCC of the MMC_2 which regulates the DC grid voltage at t=7 s, with a 200 ms fault duration. Selected simulations waveforms for scenario II are displayed in Fig. 6.

The plots for active and reactive powers displayed in Fig. 6 (a), (b), (c) and (d) show that the basic droop control method I manages to keep the active power exchange between the MMC_1 and G_1 at near zero, with real-time and offline waveforms exhibit practically identical behaviours. Fig. 6 (e) and (f) show the DC voltages and DC currents of all converter terminals, with the DC voltages across the DC grid in Fig. 1 has exhibited an increase by 9% for all converters during the AC fault. The rise of the DC voltages start at the instant of AC fault inception at PCC of MMC_2, with the DC voltages stabilised quickly as the MMC_1 that operates with droop method 1 temporarily takes over the function of DC voltage regulation, which evidently in large increase in its active power exchange with G_1 in effort to eliminate the DC power mismatch in the DC grid. Fig. 6 (b) shows that the active and reactive powers of MMC_2 that suffers AC fault have dropped to zeros, and this creates the DC overvoltage observed in Fig. 6 (e). On the other hand, the MMC_3 retains its pre-fault active power setting. Based on the results displayed in Fig. 6 (a) through (f), it can be concluded that the loss of DC voltage controlling converter MMC_2 does not mean the total loss of control over the DC voltage of the DC grid. It is worth underscoring that this simulation scenario reveals the importance of droop method 1 that enables the MMC_1 to maintain power balance within the DC grid during the AC fault. Fig. 6 (g) shows the voltage magnitudes measured at PCCs of the MMC_1, MMC_2 and MMC_3, and these plots show that the voltage at the PCC of the MMC_2 has fallen to zero during AC fault, while those of the MMC_1 and MMC_3 remain largely unaffected as expected. Fig. 6 (h) and (i), and (j) and (k) present three-phase instantaneous AC voltages and currents measured at PCC of the MMC_2, and these waveforms show that real-time and offline simulation platforms produce practically identical results.

On the basis of the results shown in Fig. 6, the following conclusions are drawn:

- The developed user-defined offline and real-time HVDC converter models which were extensively validated at converter level (RTDS and PSCAD) and offline DC grid in previous reports are well-suited for DC grid simulations.
- The user-defined converter models and associated control systems are capable of operating under complex high-level controllers such as droop control method 1 being considered in this scenario. This is achieved with the behaviours of all converter terminals being in line with the theoretical understandings that underpin the MMC operation as part of such a complex DC grid.

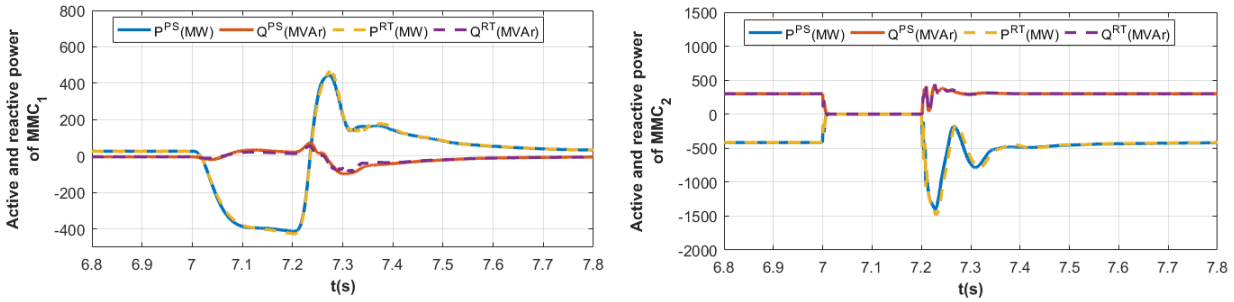
Active and reactive power of MMC1
P^PS(MW) Q^PS(MVAr) P^RT(MW) Q^RT(MVAr)
t(s)

(a)

Active and reactive power of MMC2
P^PS(MW) Q^PS(MVAr) P^RT(MW) Q^RT(MVAr)
t(s)

(b)

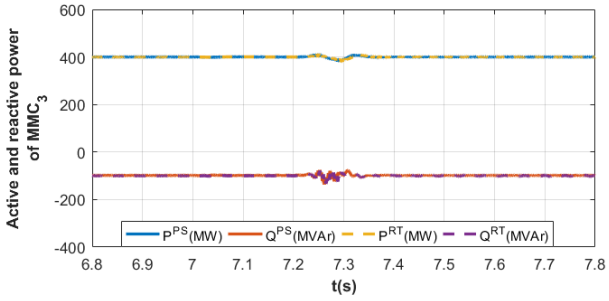
Active and reactive power of MMC3
P^PS(MW) Q^PS(MVAr) P^RT(MW) Q^RT(MVAr)
t(s)

(c)

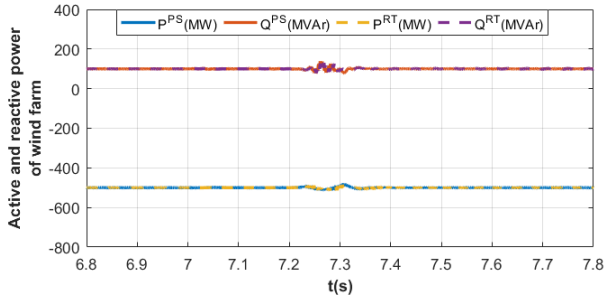
Active and reactive power of wind farm
P^PS(MW) Q^PS(MVAr) P^RT(MW) Q^RT(MVAr)
t(s)

(d)

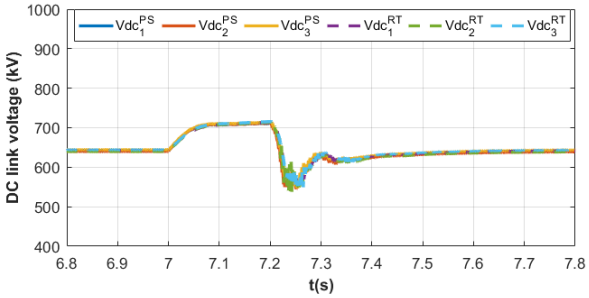
DC link voltage (kV)
Vdc1^PS Vdc2^PS Vdc3^PS Vdc1^RT Vdc2^RT Vdc3^RT
t(s)

(e)

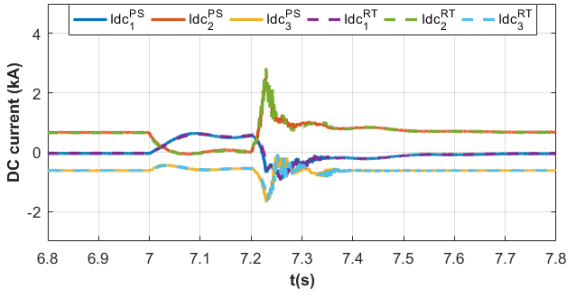
DC current (kA)
Idc1^PS Idc2^PS Idc3^PS Idc1^RT Idc2^RT Idc3^RT
t(s)

(f)

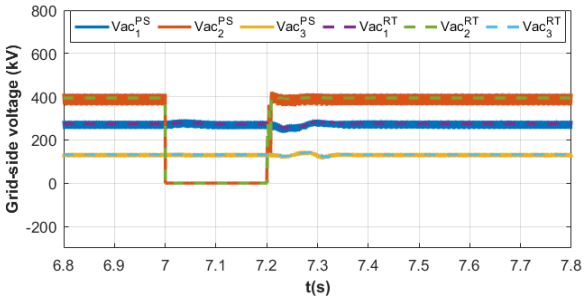
Grid-side voltage (kV)
Vac1^PS Vac2^PS Vac3^PS Vac1^RT Vac2^RT Vac3^RT
t(s)

(g)

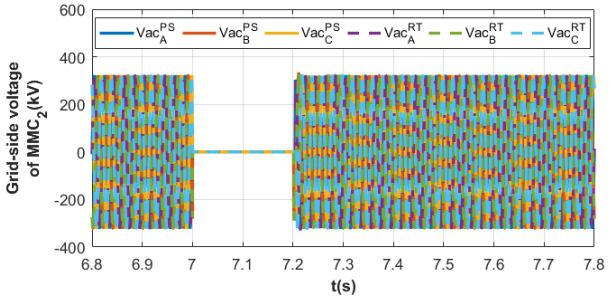
Grid-side voltage of MMC2 (kV)
VacA^PS VacB^PS VacC^PS VacA^RT VacB^RT VacC^RT
t(s)

(h)

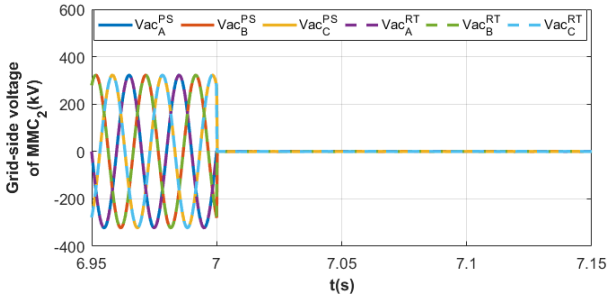
Grid-side voltage of MMC2 (kV)
VacA^PS VacB^PS VacC^PS VacA^RT VacB^RT VacC^RT
t(s)

(i)

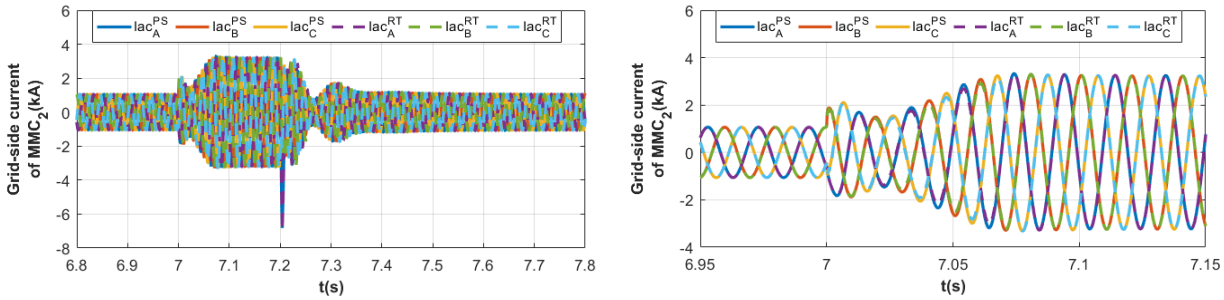

(j) (k)

Fig. 6: Real-time and offline simulation waveforms that illustrate the AC fault ride-through performance of DC grid when converter MMC_2 is subjected to an AC fault in its AC side at PCC (real-time waveforms overlaid on their offline counterparts)

3.3 Scenario III: Droop Control-Method 2

This section uses real-time and offline simulations to evaluate the performance of droop method 2 during worst-case AC fault scenario (solid three-phase AC faults at MMC_2). In this scenario, P-V_{dc} droop (denoted as droop control method) is employed at MMC_1, and AC fault is applied at t=7 s at PCC of the MMC_2. The DC grid operating conditions are summarized as follows:

- MMC_1 is equipped with P- V_{dc} droop method, denoted as droop control method 2 as shown in Fig. 3. Under normal operation, the DC voltage variation range is small and thus the method ensures the active power is controlled at the set-point (400 MW in this case). During abnormal DC voltage conditions, the active power of MMC_1 will automatically adjusted to ensure the DC voltage is regulated within a certain limit as shown in Fig. 3 (a). The local AC voltage is constantly controlled at 275 kV (line-to-line).
- In pre-fault, MMC_2 uses conventional PI based DC voltage controller to regulate the DC grid voltage constantly at 640 kV (pole-to-pole) and maintains its reactive power output constant at +300 MVAr.
- MMC_3 regulates AC voltage at its PCC at 132 kV, while the wind farm outputs -500 MW and +100 MVAr.

In this scenario, an AC fault is applied in the PCC of the MMC_2 which regulates the DC grid voltage at t=7 s, with a 200 ms fault duration. Selected simulations waveforms for scenario III are displayed in Fig. 7.

The traces for active and reactive powers displayed in Fig. 7 (a), (b), (c) and (d) show that the droop control method 2 successfully controls the active power exchange of the MMC_1 with the G_1 at +400 MW (the set point) during normal operation, with real-time and offline waveforms exhibit similar behaviours. Fig. 7 (e) and (f) show the DC voltages and DC currents of all converter terminals. The DC voltages shown indicate that droop control method 2 successfully limits the DC grid voltage during the AC fault. As in previous scenario II, the rise of the DC voltages starts at the instant of AC fault inception at PCC of MMC_2, with the DC voltages have stabilised quickly with the aid of MMC_1 taking over the function of DC voltage regulation. This is also evident from the large adjustment of its active power exchange with G_1 in effort to eliminating the DC power mismatch in the DC grid. Fig. 7 (b) shows that the active and reactive powers of the MMC_2 that suffers AC fault have plunged to zeros. On the other hand, the MMC_3 retains its pre-fault active and reactive power setting points. Based on the results displayed in Fig. 7 (a) - (f), it is concluded

that the loss of DC voltage controlling converter MMC_2 does not mean the total loss of control over the DC voltage of the DC grid, as the droop control method 2 implemented in MMC_1 is effective in ensuring rapid nullifications of the power balance during the AC fault. Fig. 7 (g) shows the voltage magnitudes measured at PCCs of the MMC_1, MMC_2 an MMC_3, which show the voltage at the PCC of the MMC_2 has fallen to zero during AC fault, while that of the MMC_1 and MMC_3 remain largely unaffected. Fig. 7 (h) and (i), and (j) and (k) present three-phase instantaneous AC voltages and currents measured at PCC of the MMC_2, and these waveforms show that the real-time and offline simulation platforms produce practically identical results.

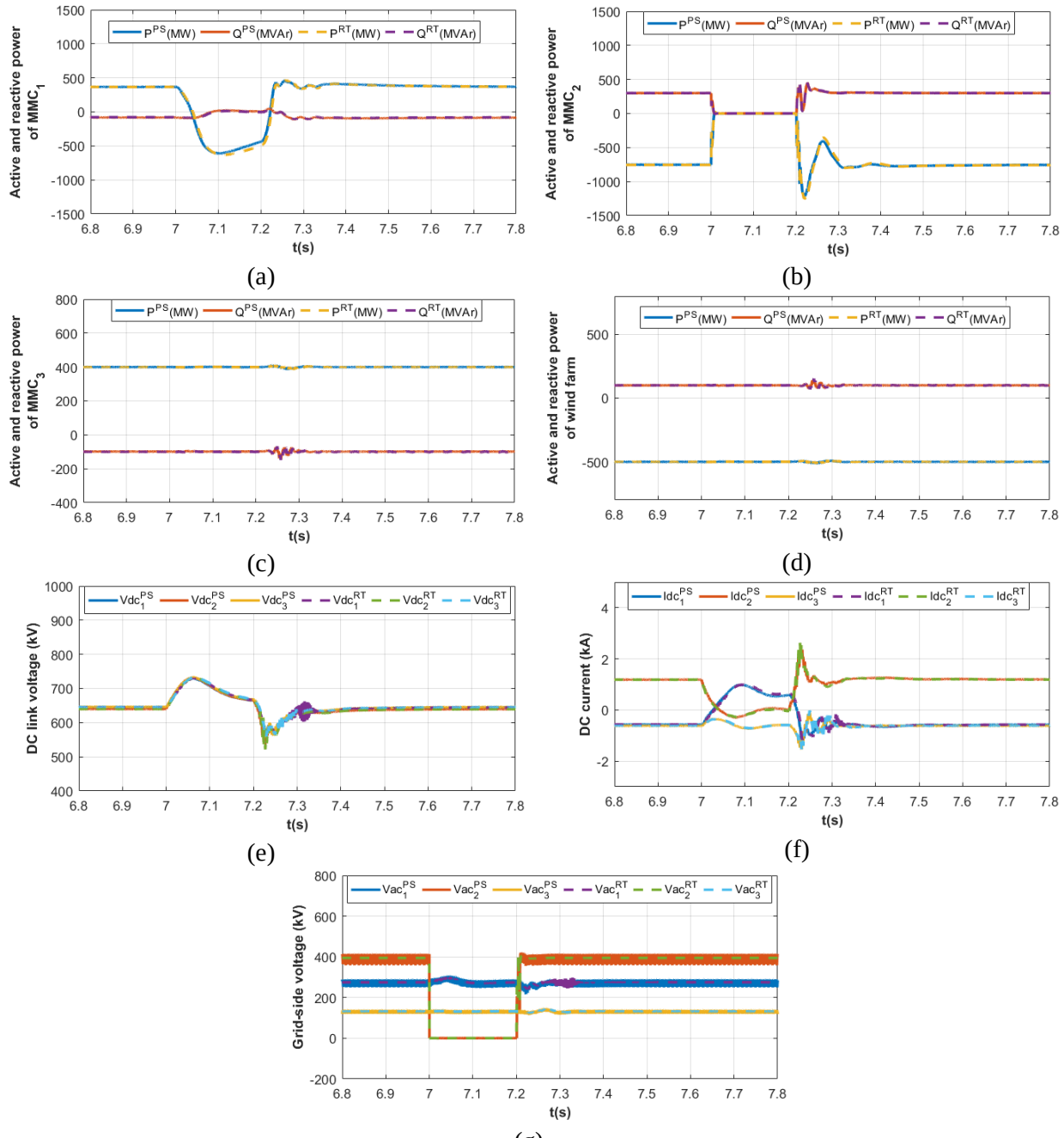

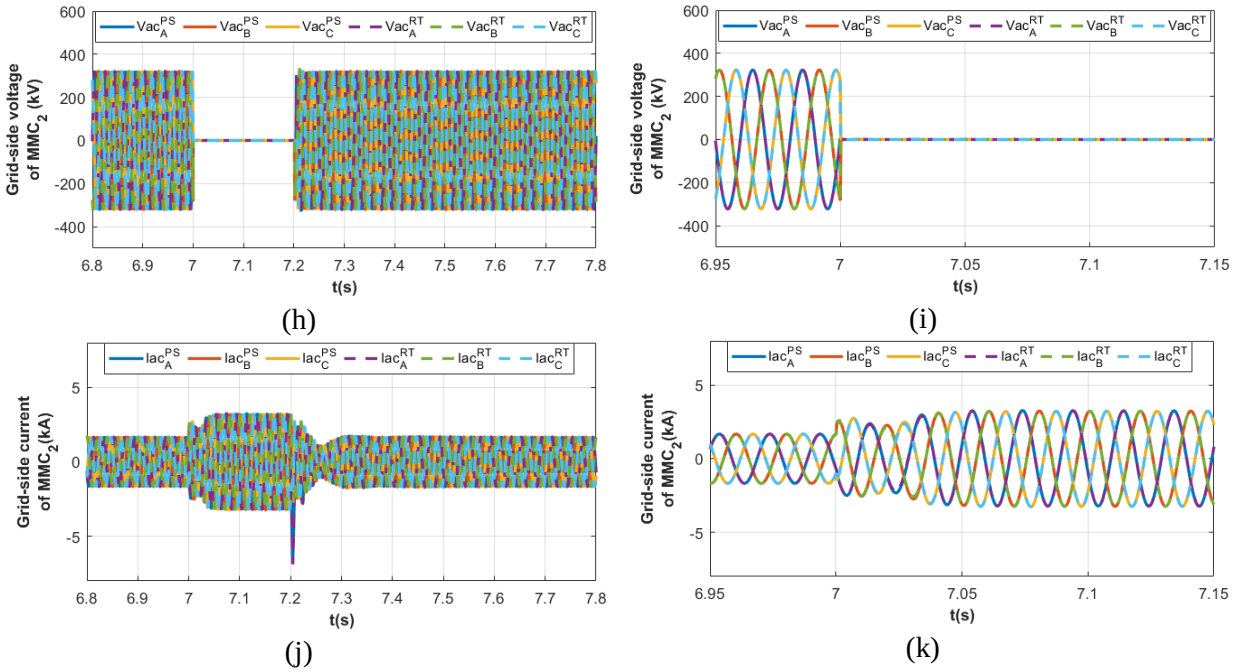

Fig. 7: Simulation waveforms that illustrate the performance of the DC grid when MMC_1 is controlled based on droop method 2 and the other DC voltage controlling converter MMC_2 is subjected to AC fault in its AC side.

4 Conclusions

This report has presented a final validation of the offline and real-time user-defined HB-MMC models and associated controllers, which were extensively validated in previous reports, but this time the emphasis is given to their applicability and suitability for complex studies in DC grids. Results of normal operation and AC faults with different droop arrangements presented in this report have indicated the robustness of these user-defined models for performing a wide range of system studies. Besides this report, the work presented in the paper submitted to ACDC2019 [7] have further confirmed the suitability, accuracy and stability of a range of converter models have been developed as part of this projects when employed complex studies, ranging from normal operation with adjustable set-points to AC and DC faults.

5 References

[1] G. Tang, Z. He, H. Pang, X. Huang, and X. p. Zhang, "Basic topology and key devices of the five-terminal DC grid," *CSEE Journal of Power and Energy Systems*, vol. 1, no. 2, pp. 22-35, 2015.

[2] H. Rao, "Architecture of Nan'ao multi-terminal VSC-HVDC system and its multi-functional control," *CSEE Journal of Power and Energy Systems*, vol. 1, no. 1, pp. 9-18, 2015.

[3] L. L. Wang Hao, and Wu Dianfeng. (2014, 27/02/2015). *'Hierarchical control in a 5-terminal VSC-HVDC project'*. Available: http://www.ee.co.za/article/hierarchical-control-5-terminal-vsc-hvdc-project.html

[4] L. Tang, "Control and Application of Multi-terminal HVDC based on voltage-Source Converter," Doctor of Philosophy, Electrical and Computer Engineering, McGill University, Montréal, Québec, Canada, 2003.

[5] K. Rouzbehi, A. Miranian, A. Luna, and P. Rodriguez, "DC Voltage Control and Power Sharing in Multiterminal DC Grids Based on Optimal DC Power Flow and Voltage-Droop Strategy," *IEEE Journal of Emerging and Selected Topics in Power Electronics*, vol. 2, no. 4, pp. 1171-1180, 2014.

[6] L. Xu, L. Yao, M. Bazargan, and Y. Wang, "The Role of Multiterminal HVDC for Wind Power Transmission and AC Network Support," in *Power and Energy Engineering Conference (APPEEC), 2010 Asia-Pacific*, 2010, pp. 1-4.

[7] TR on Offline DC grid model development, *Strathclyde-UK National HVDC Centre collaborative research project*, TR ref. USTRATH-HVDC Centre-P1-003, September 2018.

[8] D. Guo *et al.*, "Interoperability of Different Voltage Source Converter Topologies in HVDC Grids," presented at the 15th IET International Conference on AC and DC Power Transmssion Systems, Coventry, UK, 5-7 Feb, 2019.